Castrichini, A., Hodigere Siddaramaiah, V., Calderon, D., Cooper, J., Wilson, T., & Lemmens, Y. (2017). Preliminary investigation of use of flexible folding wing tips for static and dynamic load alleviation. Aeronautical Journal, 121(1235), 73-94. DOI: 10.1017/aer.2016.108

Preliminary Investigation of Use of Flexible Folding Wing-Tips for Static and Dynamic Loads Alleviation

A. Castrichini[1], V. Hodigere Siddaramaiah[2], D.E. Calderon[2], J.E. Cooper[3]
University of Bristol, Bristol, BS8 1TH, United Kingdom

T. Wilson[4]
Airbus Operations Ltd., Filton, BS99 7AR, United Kingdom

Y. Lemmens[5]
Siemens, Leuven, Interleuvenlaan 68 B-3001, Belgium

A recent consideration in aircraft design is the use of folding wing-tips with the aim of enabling higher aspect ratio aircraft with less induced drag, but also meeting airport gate limitations. This study investigates the effect of exploiting folding wing-tips in-flight, as device to reduce both static and dynamic loads. A representative civil jet aircraft aeroelastic model was used to explore the effect of introducing a wing-tip device, connected to the wings with an elastic hinge, on the loads behavior. For the dynamic cases, vertical discrete gusts and continuous turbulence were considered. The effect of hinge orientation, stiffness, damping and wing-tip weight on the static and dynamic response was investigated. It was found that significant reductions in both the static and dynamic loads were possible. For the case considered, a 25% increase in span using folding wing-tips resulted in almost no increase in loads.

Nomenclature

Symbols

c_{wt}	=	Wing-tip mean chord
$C_{m\theta}$	=	Aerodynamic moment coefficient
D_{aero}	=	Hinge aerodynamic damping
D_θ	=	Hinge structural damping
f	=	Natural frequency
H	=	Gust gradient
$I_{\theta aero}$	=	Aerodynamics moment of inertia
$I_{\theta wt}$	=	Wing-tip's moment of inertia
K_{aero}	=	Hinge aerodynamic stiffness
K_θ	=	Hinge structural stiffness
L_g	=	Gust length
S_{wt}	=	Wing-tip area
V	=	Flight speed
W_g	=	Gust velocity
W_{g0}	=	Peak of the gust velocity
W_{ref}	=	Reference gust velocity
α_{WT}	=	Wing-tip angle of attack
Λ	=	Hinge orientation angle
θ	=	Wing-tip folding angle
ξ_n	=	Modal damping
Φ	=	Von Karman PSD
ψ_n	=	Random phase

Abbreviations

FWT	=	Folding Wing-Tip
PSD	=	Power Spectral Density
RMS	=	Root Mean Square
WRBM	=	Wing Root Bending Moment

[1] Research Engineer, Aerospace Competence Centre

[2] Postdoctoral Research Assistant

[3] Airbus Royal Academy of Engineering Sir George White Chair in Aerospace Engineering

[4] Head of Technical Capability for Aircraft Loads Flight Physics

[5] Project Leader RTD, Aerospace Competence Centre

I. Introduction

Much effort have been made to design aircraft in order to optimize fuel consumption through reduction of aerodynamic drag. A sizable contribution to the overall drag is lift-induced drag, which could be reduced by increasing the wingspan, but such a design solution has well defined limits imposed by the maximum aircraft dimensions allowed at airports and also the increase in bending moments along the wing. A possible solution to the first issue is the use of folding wings that can be employed on the ground in a similar way to the retractable wings used on aircraft carrier borne aircraft. An example of this approach relevant to civil applications is the latest version of the B-777 which will have a folding wing capability to be activated during taxing to and from the gates. The inclusion of such a design feature raises the question as to whether such a folding device could also be used to enable loads reduction on the aircraft during the flight.

This work is aimed at studying the benefits of using a flexible wing-fold device for loads alleviation and considering how it would be implemented on civil jet aircraft. The main idea consists of introducing a hinge in order to allow the wing-tips to rotate, as shown in Fig. 1. The orientation of the hinge line relative to the airflow is a key parameter to enable successful loads alleviation. When the hinge line is not parallel to the free stream, but is rotated outboard as in Fig. 1(b, d), folding the wing-tip up introduces a decrease in the local angle of attack. Knowing the hinge orientation Λ and the angle of rotation of the wing-tip θ, the local angle of attack $\Delta\alpha_{WT}$ can be shown to be given by

$$\alpha_{WT} = -\tan^{-1}(\tan\theta \sin\Lambda) \tag{1}$$

Such an effect implies that using a non-zero hinge angle provides a means to reduce the loads acting on the wing, leading to the possibility of achieving a wing-tip extension with limited or even minimal impact on wing weight.

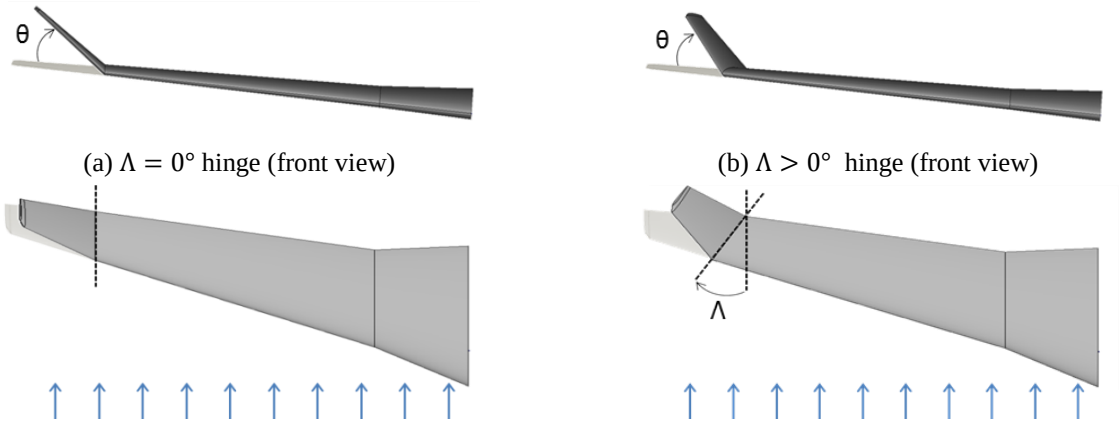

(a) $\Lambda = 0°$ hinge (front view)

(b) $\Lambda > 0°$ hinge (front view)

(c) $\Lambda = 0°$ hinge (top view)

(d) $\Lambda > 0°$ hinge (top view)

Figure 1. Hinge Orientations

A series of numerical simulations are performed on a representative civil aircraft model to demonstrate the benefits of loads reduction on static and dynamic gust loads though the use of a folding wing-tip.

II. Aeroelastic Model

A. Structural Modeling

Figure 2 shows the baseline aeroelastic model used for the analyses, which was a modified version of the FFAST aeroelastic model [1] of a representative civil jet aircraft, whose structure was modelled using a "stick" model with lumped masses. The main objective was to investigate the possibility of having an aircraft configuration which enables a higher aspect ratio, and consequent reduction in the induced drag, whilst limiting the increase in loads (especially in terms of wing bending moment) experienced by the aircraft, thus keeping the structure as light as possible. The baseline model, without wing-tips, Fig. 2, was considered as the reference to evaluate the effect of using the folding wing-tips, also shown in Fig. 2, which were attached to the structure using a flexible hinge, giving

an increase in span of 25% compared to the baseline. Figure 3 shows a detailed view of the structural model with the attached wing-tip device.

The hinge was modeled by constraining two coincident nodes, one belonging to the main airframe and the other to the wing-tip, to have the same translations but free to have different relative rotations with respect to the pre-defined hinge axis. The linear structural model did not account for the wing-span shortening effect due to the wing-tip rotations, but this effect was considered to be negligible.

To investigate the effects of such a hinge device on the aircraft response, several structural configurations were analyzed by varying both the orientation of the hinge with respect to the free stream direction, 0° and 25°, and the weight of each wing-tip. A 943Kg mass configuration was defined in order to have the same structural configuration used in a previous work [2], while the other configurations were introduced to examine the effect of varying the wing-tip mass. Several values for the spring torsional stiffness and damping were also investigated for each configuration, starting from a fixed hinge up to an almost free hinge (a small stiffness was used to avoid numerical singularities).

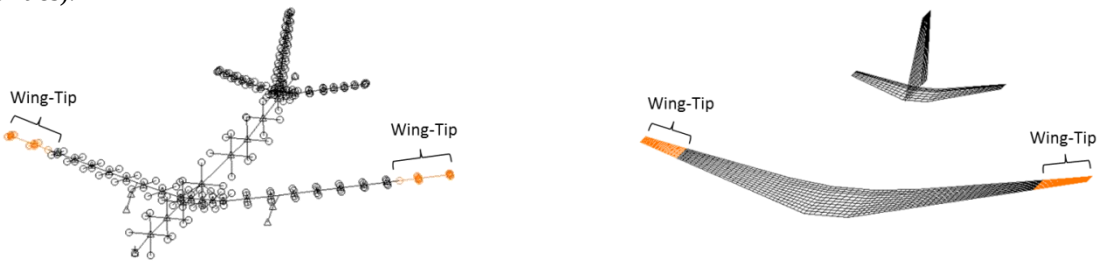

(a) Structural model (b) Aerodynamic model

Figure 2. Aeroelastic Model Showing Baseline Model and Wing-Tips

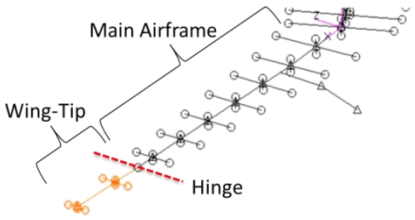

Figure 3. Folding Wing-Tip Modeling Detail

B. Aerodynamic Modeling

The Doublet Lattice panel method [3, 4] was used for the aerodynamic model, which is based upon linear unsteady potential flow theory, making the assumptions of inviscid, irrotational, compressible and attached flow, subject to small angle of attack or side slip. As a consequence, nonlinear aerodynamic effects such as flow separations, shocks, turbulence, boundary layers as well as aerodynamic drag were not accounted for. Only the lift forces and pitching moment, defined for each aerodynamic panel, were considered in the aerodynamic loads estimation. A further limitation, due to the small angle of attack or side slip assumption, is that the aerodynamic forces do not to change their direction as a function of the actual deformation of the structure and wing-tip deflection. The aerodynamic forces were defined with respect to the local normal direction of each panel by modifying the modulus, but not the orientation, of each aerodynamic force as a function of the local deformation.

The above approximations are general acceptable when applied to conventional aircraft structures subject to small deformations, and indeed the Doublet Lattice method has been the aeroelastic workhorse of the aerospace industry for over 40 years. Within an industrial environment, aircraft loads estimation requires the computation many tens of thousands of loads cases and as a consequence, high fidelity CFD based analyses cannot be extensively employed. Furthermore unsteady gust analyses using CFD models is still a novel methodology and is very much an immature approach for industrial applications and consequently the Doublet Lattice method is still a standard tool within the industrial community for aircraft loads estimation.

Although modeling of the follower aerodynamic forces effects might be required when considering folding wing-tips, the results reported in the following sections show that the wing-tip deflections are in general quite limited. Consequently, it has been considered acceptable to use the Doublet Lattice approach for this preliminary

investigation to determine a qualitative analysis of the effect of the folding wing-tip on aircraft loads and dynamic response. A high fidelity estimation of the aerodynamic properties of such device is well beyond the purpose of this work and will be tackled in future research activities along with wind tunnel testing.

III. Aeroelastic Analyses

In order to investigate the effects of the wing-tip device with different parameter settings, several aeroelastic analyses have been made for different structural and flight configurations.

A. Static Trim Solution

A static aeroelastic analysis was performed using Nastran SOL 144. A "1-g" load case was considered with the aircraft operating at M=0.6 at 25000 ft, equivalent to a dynamic pressure of 9.47KPa. The aircraft was left free to pitch and plunge in order to achieve the trim configuration by considering the angle of attack and the elevator deflection as trim variables.

B. Flutter Analysis

The dynamic stability of the aeroelastic system was verified through a flutter analysis performed using the 'PK' and 'PKNL' methods in Nastran SOL 145. The following analyses were performed:

- A matched configuration analysis where the number of Mach was fixed to a cruise value of M=0.82 and the velocity changes, from 241.9m/s to 274.83m/s, as a function of the altitude from 4500 ft to 50000 ft.
- Three unmatched configuration analyses where the velocity was swept from 100 m/s to 900 m/s at the following flight configurations: M=0.4 at altitude 20000 ft; M=0.6 at altitude 25000 ft; M =0.8 at altitude 30000 ft. The authors are aware that the flight speeds considered for the unmatched analyses were beyond the normal flight envelope limits; nevertheless they were used in the flutter calculation with the purpose of highlighting the qualitative trend of the aircraft flutter behavior by varying the different design parameters.

The selected modal base included modes in the frequency range (0. 12.] Hz with a modal damping of 2.%, while the rigid body modes were removed from the analysis since they have little damping and oscillate around the zero damping level, often causing a false flutter speed reading.

C. "1-cosine" Gust Response Analysis

In this study, the aircraft was subjected to a discrete gust in the form of a "1-cosine" gust, using Nastran SOL 146 such that the velocity profile acted in a vertical direction normal to the path of the aircraft.
The gust profile was defined as

$$w_g(t) = \frac{w_{g0}}{2}\left(1 - \cos\frac{2\pi Vt}{L_g}\right) \tag{2}$$

where L_g is the gust length (twice the gust gradient H), V is the flight speed in TAS and w_{g0} peak gust velocity. The latter defined by

$$w_{g0} = w_{ref}\left(\frac{H}{106.17}\right)^{\frac{1}{6}} \tag{3}$$

where w_{ref} was varied linearly from 13.4 m/s EAS at 15000 ft to 7.9 m/s EAS at 50000 ft, based on the FAA Federal Aviation and EASA Regulations [3]. At the investigated flight altitude of 25000 ft and Mach number of M=0.6, the gust reference velocity is 11.48 m/s EAS, while the gust lengths was varied between 18 m and 214 m. For this analysis a value of Δf = 0.04166 Hz was selected as frequency resolution and 600 frequency increments were defined to cover the frequency range from 0. Hz to 25. Hz.

D. Continuous Turbulence Response Analysis

A continuous turbulence gust case was also investigated. According FAA Federal Aviation and EASA Regulations [3], for the same flight point of the deterministic gust analyses, the reference turbulence intensity is taken as 24.08 m/s TAS. A Von Karman power spectral density of the atmospheric turbulence with a scale of turbulence of 2500 ft was considered.

For this analysis a value of $\Delta f = 0.005$Hz was selected as frequency resolution and 5000 frequency increments were defined to cover the frequency range from 0. Hz to 25. Hz. The Root Mean Square (RMS) of the response (area of the Power Spectral Density (PSD)) was considered as the means to determine the effect of the various hinge parameters.

IV. Results

A. Static Aeroelastic Trim Solution

In this section, the static aeroelastic longitudinal trim solution of the extended wing-tip aircraft is shown. Figures 4 and 5 show the trim angle of attack and the bending moment distribution along the spanwise direction respectively, for the 0° and 25° flexible hinges. The hinge stiffness corresponds to the rotational stiffness about the axis that runs through the hinge line, which was varied between 1.E0 Nm/rad and 1.E10 Nm/rad such that the highest stiffness considered in this study corresponded to a fixed hinge.

The results show a number of differences in the response between the baseline model and the model with folding wing-tips. There were almost no differences between the static responses of the models with different wing-tip weights, as would be expected for a static aeroelastic results; however, the response of the model was highly influenced by the orientation of the hinge.

(a) 943 Kg wing-tip model

(b) 100 Kg wing-tip model

Figure 4. Static Trim Angle Of Attack
(–■–:fixed hinge model; –●–:baseline model; –◆–:25° hinge model; –▲–:0° hinge model)

- 0° hinge model:
  The introduction of a 0° elastic hinge did not introduce any difference in the response with respect to the fixed hinge model. The deflection of the wing-tip did not generate any variation in the local angle of attack since the folding motion does not have any pitching component, meaning that the aerodynamic forces were the same as the fixed hinge model. Using a hinge spring with a stiffness lower than 1.E06 Nm/rad led to a divergence solution due to very high rotation of the outer wing, and was thus ignored.
- 25° hinge model:
  The baseline and the fixed hinge models represented the lower and upper boundaries of the elastic hinge model's response. The lower was the hinge stiffness, the higher the wing-tip rotation and so the lower the lift given by the rotated wing-tip. The wing-tip rotation gave a decrease in the lift contribution thus reducing the loads (bending moment and vertical shear) experienced by the aircraft. The more the wing-tip was rotated, the higher the required trim angle of attack since the inner wing had to generate more lift to balance the aircraft's weight. It is possible to use a very low structural stiffness for the hinge since the wing-tip behavior is characterized also by an "aerodynamic stiffness" contribution. The most efficient loads alleviation was achieved for the 100 Kg wing-tip model with a spring stiffness of 1.E0 Nm/rad, where the wing root bending moment was just 4.36% higher than the baseline model with no wing-tip. For this case, the wing-tip rotation of θ=26.67° led to a decrease in the local angle of attack of $\Delta\alpha$=-11.98°, which corresponded to an effective angle of attack of α=-5.20°, giving a global angle of attack at the trim configuration of α= 6.78°.

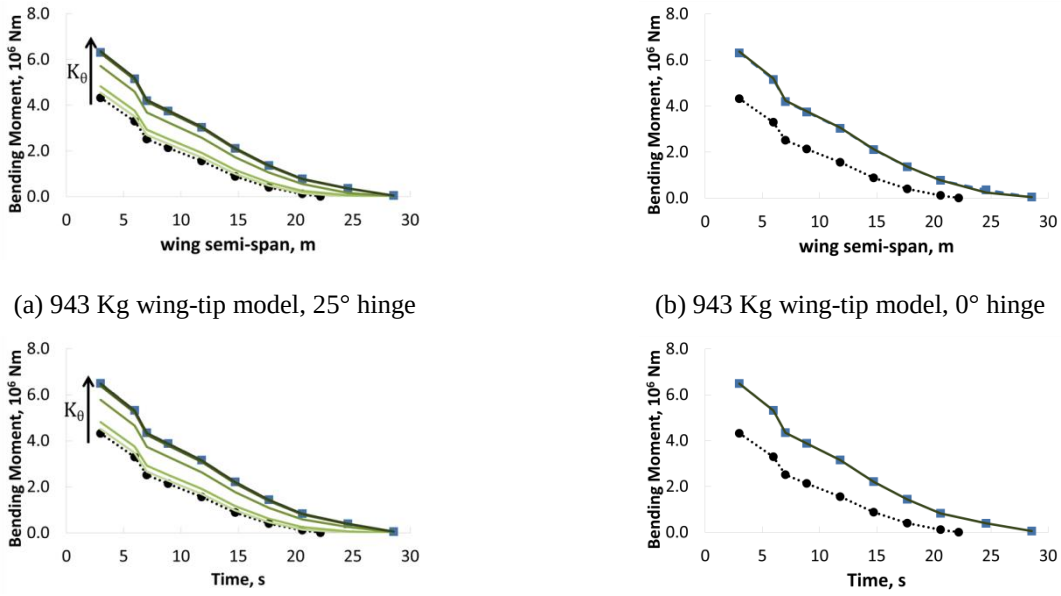

(a) 943 Kg wing-tip model, 25° hinge

(b) 943 Kg wing-tip model, 0° hinge

(c) 100 Kg wing-tip model, 25° hinge

(d) 100 Kg wing-tip model, 0° hinge

Figure 5. Wing Bending Moment Distribution
(-■-:fixed hinge model; −●−:baseline model; ——:flexible hinge model
K_θ=[1.E0, 1.E5, 1.E6, 1.E7, 1.E8] Nm/rad)

B. Flutter Analysis

A flutter analysis was performed for different flight configurations, hinge directions, wing-tip weight and spring stiffness; no hinge damping was defined on the model in order to have a more conservative evaluation of the stability boundaries.

The normal mode analysis showed that when the hinge stiffness was higher than 1.E07Nm/rad the mode shapes and modal frequencies were almost the same of the fixed hinge model. The use of a more flexible spring gave changes in the modal characteristics affecting mainly the lower frequencies (< 4.Hz). For hinge stiffness values lower than 1.E04Nm/rad the first two flexible modes represented a local symmetric and antisymmetric wing-tip folding, respectively, while the other modes involved interactions between the wing-tip and the main airframe.
Figure 6 and 7 show the stability boundaries of the wing-tip models over a range of hinge stiffness and wing-tip mass values.

- 25° hinge.
  The flutter analyses showed how high spring stiffness values and low wing-tip mass were beneficial for the stability of the aeroelastic system leading to high flutter velocities. The wing-tip mass was the most influential design parameter affecting the flutter speed, in fact for values lower than 300 Kg the sensitivity of the flutter speed with respect the spring stiffness was negligible.
  Figures 7(a), 7(b) and 8 show the V-g and V-ω plots for an unmatched analysis (M=0.6, at 25000ft) and the main components of the critical eigenvector for the 943 Kg wing-tip with a spring stiffness of 1.E0 Nm/rad; the flutter mechanism is driven by a coupling of the first symmetric wing-tip mode with the first symmetric bending mode of the wing with the wing-tips shifted in phase of 180°. This coupling is also enhanced by the fact that the bending of the wing-tip introduces a variation of the local angle of attack which does not occur for the 0° hinge model. When a heavy wing-tip is employed, M>400 Kg, increasing the spring stiffness is beneficial. For spring stiffness higher than 1.E06Nm/rad, the local wing-tips modes were not present any more leading to a variation of the flutter mechanism and to higher flutter speeds with respect the more flexible case.
  Figure 7(c) and 7(d) show the same V-g and V-ω plots as in the previous case, but now for a 100 Kg wing-tip with a spring stiffness of 1.E0 Nm/rad. It can be seen in Fig. 7(c) the two poles that are highly damped have the main components of the complex eigenvectors given by the first two wing-tip modes. The wing-tip modes, that caused the instability problems for the previous case, are now more stable as the velocity increased due to the increment of the aerodynamic stiffness and reduction in the inertia of the wing-tips with respect to the 943Kg model. Figure 7(d) shows that the poles, that represent the local modes of the wing-tips, had a

frequency growing almost linearly with the speed (true for K_θ<1.E06Nm/rad). The higher was the flight speed, the larger was the contribution of the aerodynamic stiffness on the hinge global stiffness (structural + aerodynamic) leading to an increase in the wing-tip mode natural frequency. This linear trend indicates that the local wing-tip modes tended to remain mostly uncoupled from the main airframe modes when a low wing-tip mass and low hinge spring stiffness were defined. The local wing-tip dynamic response can be modelled, as first approximation, as a single degree of freedom system such that

$$\begin{gathered}(I_{\theta wt} + I_{\theta aero})\ddot{\theta} + (D_\theta + D_{aero})\dot{\theta} + (K_\theta + K_{aero})\theta = 0 \\ I_{\theta wt}\ddot{\theta} + (D_\theta + D_{aero})\dot{\theta} + K_{aero}\theta = 0\end{gathered} \tag{4}$$

Assuming $I_{\theta aero} \ll I_{\theta wt}$ and $K_\theta < 1.E06$ (i.e. $K_\theta \ll K_{aero}$), then defining the aerodynamic stiffness as $K_{aero} = \frac{1}{2}\rho V^2 s_{wt} c_{wt} C_{m\theta} \sin\Lambda$, the natural frequency of the wing-tip is given by

$$f \approx \frac{1}{2\pi}\sqrt{\frac{K_{aero}\left(1-\xi_n{}^2\right)}{I_{\theta wt}}} = \frac{V}{2\pi}\sqrt{\frac{\frac{1}{2}\rho s_{wt} c_{wt} Cm_\theta \sin\Lambda\left(1-\xi_n{}^2\right)}{I_{\theta wt}}} \tag{5}$$

- 0° hinge.
  All the analyses that were undertaken, both with matched and unmatched flight points, exhibited an overall stable behavior across the entire range of the analyzed flight points with very high flutter velocities. Four hinge stiffness values were considered: 1.E06 Nm/rad, 1.E07 Nm/rad, 1.E08 Nm/rad, 1.E12 Nm/rad. For the two stiffer springs the flutter speeds had the same trend of the 25° hinge model with the same stiffness values, as in Fig. 6, being the hinge nearly rigid. A change in the stability of the system for the 0° hinge model was observed when the two softer springs were defined. Even though statically the wing-tips deflections did not generate any variation of the aerodynamic forces, from a dynamic point they introduced an aerodynamic damping contribution which was beneficial for the flutter behavior.

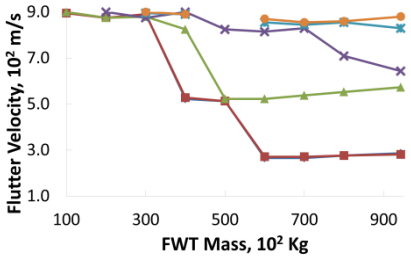

(a) Unmatched Analysis M=0.4

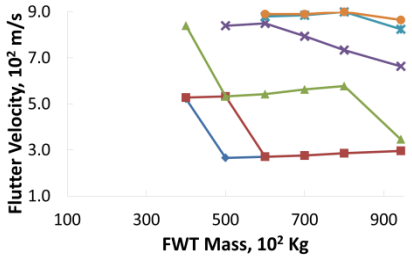

(b) Unmatched Analysis M=0.6

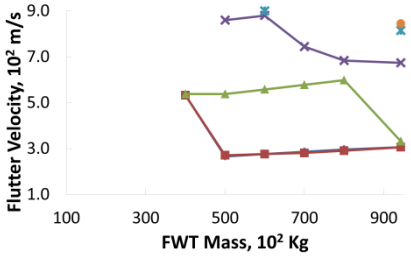

(c) Unmatched Analysis M=0.8

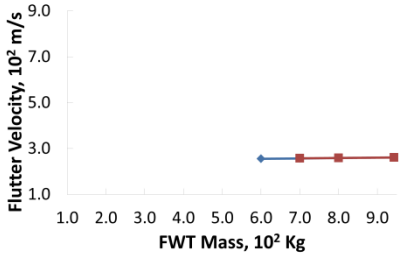

(d) Matched Analysis

Figure 6. 25° Hinge Model, Flutter Velocities
(: K_θ=1.E0Nm/rad; : K_θ=1.E5Nm/rad; : K_θ=1.E6Nm/rad; : K_θ=1.E7Nm/rad; : K_θ=1.E8Nm/rad; : K_θ=1.E12Nm/rad;)

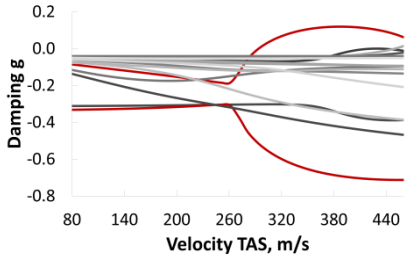

(a) 943 Kg wing-tip model, V-g

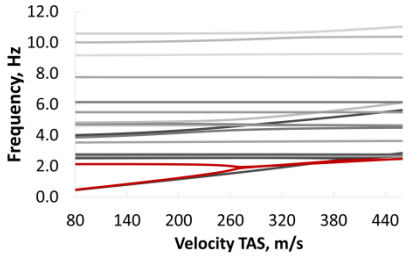

(b) 943 Kg wing-tip model, V-ω

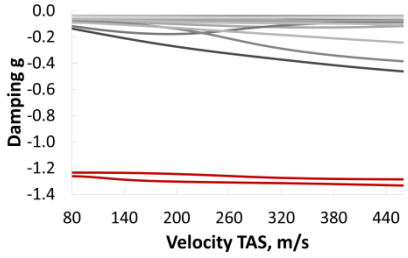

(c) 100 Kg wing-tip model, V-g

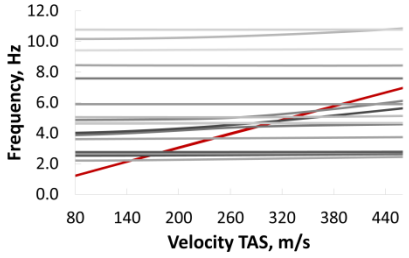

(d) 100 Kg wing-tip model, V-ω

Figure 7. 25° Hinge Model, K_θ=1.E0 Nm/rad – Unmatched Analysis V-g V-ω Plots

(a) Mode 1.

(b) Mode 3.

Figure 8. Main Modal Components Of The Critical Eigenvector

1. Hinge Damping Effect

Further investigations were made to determine the effect on the stability boundaries of the model by introducing a local damper element on the hinge. These analyses were carried out only for the 25° hinge model with a spring stiffness of 1.E0 Nm/rad, varying the value of the damping element from 1.E03Nms/rad to 1.E06Nms/rad.
The flutter speeds are shown in Fig. 9 and as might be expected, the flutter velocities were higher for larger values of the damping element. For D_θ=1.E06Nms/rad the first two modes (which correspond to the local wing-tip folding modes) are critically damped and possess a zero frequency for all the velocities of the analyzed flight envelope.

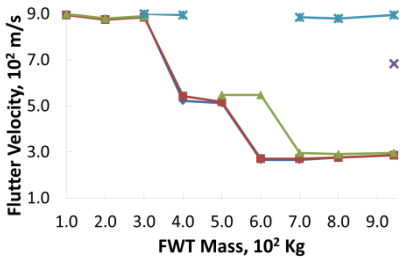

(a) Unmatched Analysis M=0.4

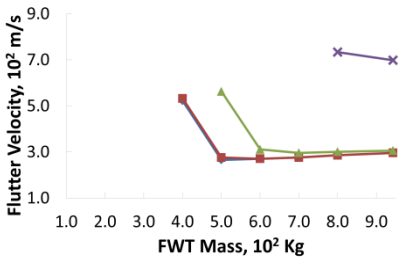

(b) Unmatched Analysis M=0.6

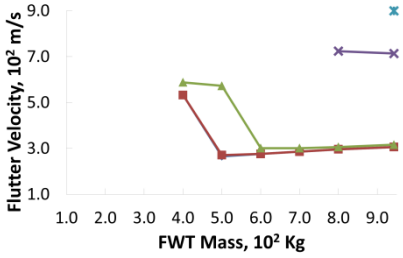

(c) Unmatched Analysis M=0.8

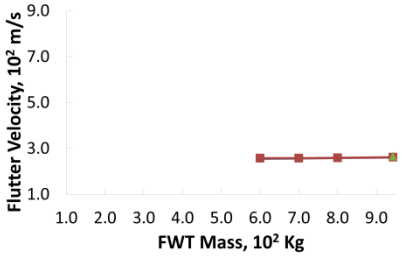

(d) Matched Analysis

Figure 9. 25° Hinge Model, Flutter Velocities – Hinge Damping Effects (K_θ= 1.E0 Nm/rad)
(: D_θ=1.E0Nms/rad; : D_θ=1.E3Nms/rad; : D_θ=1.E4Nms/rad; : D_θ=1.E5Nms/rad; : D_θ=1.E6Nms/rad)

C. "1-cosine" Gust Response Analysis

1. Hinge Stiffness Effect

In this section, the dynamic response of the model with the folding wing-tips during a gust event was considered for a linear spring added to the hinge with no local damper. Figure 10 shows the maximum and minimum incremental wing root bending moments for the 100 Kg and 943 Kg wing-tip models with 0° and 25° hinge over a range of gust lengths:

- The baseline model is subjected to the lowest loads, both in terms of minimum and maximum peaks.
- 0° Hinge:
  943 Kg wing-tip model. - The introduction of the folding wing-tips enabled alleviation of the maximum positive loads with respect to the fixed hinge model, but they still remained higher than those of the baseline model. When the spring stiffness was 1.E06Nm/rad, the negative wing root bending moment was lower than that of the baseline model for the shorter gust lengths, but higher for longer gust lengths.
  100 Kg wing-tip model. - The loads remained almost the same as the fixed hinge model with varying hinge stiffness, as for the static analysis. This behavior is due to the fact that the variation of the aerodynamic forces given by the wing-tip motion did not affect the model response and the inertial forces were negligible.
- 25° hinge:
  943 Kg wing-tip model. - The maximum positive loads were experienced by the fixed hinge model. For the flexible hinge model there was a decrease in the positive loads trend with decreasing spring stiffness. However, the load alleviation effect given by the folding wing-tip was not enough to reach the loads experienced by the baseline model. When the spring stiffness had values lower than 1.E05Nm/rad, the absolute negative loads became even higher than the fixed hinge model.
  100 Kg wing-tip model. - It can be seen that both for the maximum and the minimum loads decreased with a reduction in the hinge spring stiffness.
- For all configurations, the model behaved as a fixed hinge model for spring stiffness higher than K_θ=1.E07Nm/rad.

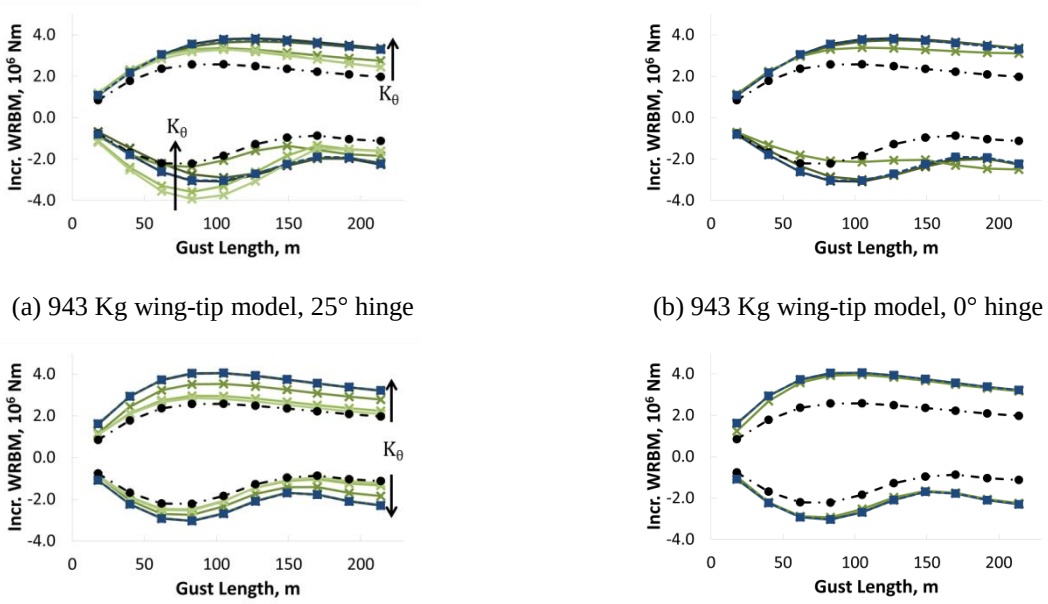

(a) 943 Kg wing-tip model, 25° hinge

(b) 943 Kg wing-tip model, 0° hinge

(c) 100 Kg wing-tip model, 25° hinge

(d) 100 Kg wing-tip model, 0° hinge

Figure 10. Wing Bending Moment Envelopes
(-■-:fixed hinge model; −●−:baseline model; ——:flexible hinge model
K_θ=[1.E0, 1.E5, 1.E6, 1.E7, 1.E8] Nm/rad)

2. Wing-Tip Mass Effect

The differences between the response of the 943Kg and 100Kg wing-tip models can be explained by looking at the time histories of the wing root bending moment for the various configurations. For this investigation, a spring stiffness of K_θ=1.E06 Nm/rad was considered for the 0° hinge, while K_θ=1.E0 Nm/rad and K_θ=1.E06 Nm/rad were considered for the 25° hinge case. In both cases there was no local damping element on the hinge. Only one gust length was considered, L_g=127 m, which was the one that, in general, produced the highest wing root loads. Figure 11 and Table 1, show the time histories of the wing root bending moment and the variation of the maximum and minimum loads with respect to the baseline model for all configurations:

- 0° Hinge:
  943 Kg wing-tip model. - The folding tip device was not able to alleviate the loads enough to reach the wing root bending moment of the baseline model. Figure 12(a) shows that the forces generated by the folding tip device were primarily given by the inertial contribution. The aerodynamic forces were lower since the wing-tip rotation did not introduce any variation on the local angle of attack; they were mainly due to the aerodynamic damping effect. There could be some alleviation effect, but this was generally unpredictable since the wing-tip behaved as an oscillating mass rather than a passive aerodynamic loads alleviation system.
  100 Kg wing-tip model. – This case did not provide much load alleviation effect and the time history of the wing root bending moment was almost unchanged with respect to the fixed hinge model. Figure 13(a) shows that the inertial forces due to the wing-tip motion were negligible with respect to the aerodynamic forces, which were slightly influenced by the wing-tip folding. Consequently, the global forces generated by the folding device were almost the same of the ones for the fixed hinge model.

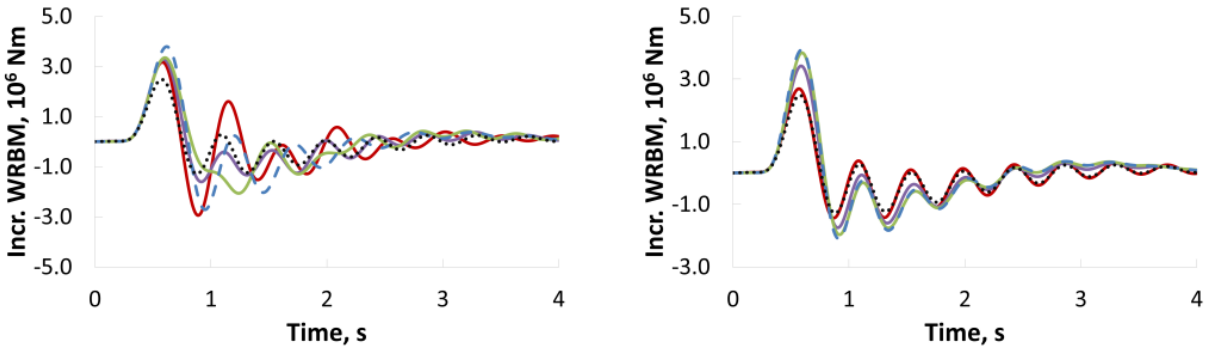

(a) 943 Kg wing-tip model (b) 100 Kg wing-tip model

Figure 11. Wing Root Bending Moment Time Histories
(– – – –:fixed hinge model; ·····: baseline model; ——: 0° hinge model K_θ=1.E6Nm/rad; ——: 25° hinge model K_θ=1.E6Nm/rad; ——: 25° hinge model K_θ=1.E0Nm/rad)

943Kg WT:	Fixed Hinge	0° Hinge K = 1.E06Nm/rad	25° Hinge K = 1.E06Nm/rad	25° Hinge K = 1.E0Nm/rad
Max. WRBM	+52.81%	+34.96%	+32.13%	+27.82%
Min. WRBM	+111.55%	+60.70%	+24.67%	+129.38%

100Kg WT:	Fixed Hinge	0° Hinge K = 1.E06Nm/rad	25° Hinge K = 1.E06Nm/rad	25° Hinge K = 1.E0Nm/rad
Max. WRBM	+52.27%	+54.44%	+37.63%	+8.34%
Min. WRBM	+63.87%	+53.59%	+36.01%	+11.97%

Table 1. Variation Of The Maximum And Minimum WRBM With Respect The Baseline Model

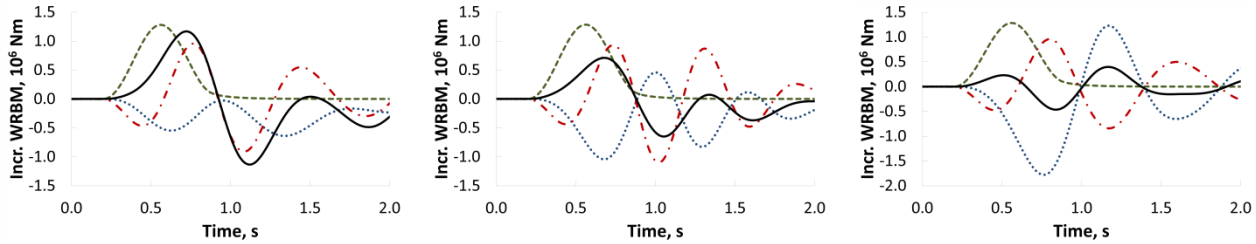

(a) 0° hinge, K_θ =1.E06 Nm/rad (b) 25° hinge, K_θ =1.E06 Nm/rad (c) 25° hinge, K_θ =1.E0 Nm/rad

(– – – –: gust loads; ·····: aerodynamic loads due to the wing-tip deflection; – · – –: inertial loads; ——: global loads)

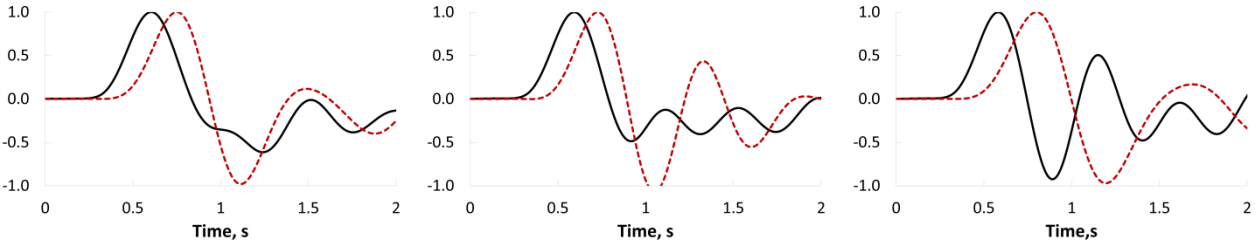

(d) 0° hinge, K_θ =1.E06 Nm/rad (e) 25° hinge, K_θ =1.E06 Nm/rad (f) 25° hinge, K_θ =1.E0 Nm/rad

(——: WRBM; – – – –: Folding Angle)

Figure 12. 943 Kg Wing-Tip Model - Upper Plots: Aerodynamic And Inertial Loads Contributions Of The Wing-Tip To The Global Wing Root Bending Moment. Lower Plots: Global Wing Root Bending Moment VS Wing-Tip Folding Angle (normalized)

- 25° Hinge:
  943 Kg wing-tip model. - For both the hinge stiffness values, the folding tip device was not able to alleviate the loads enough to reach the wing root bending moment levels of the baseline model. Although the first positive peak for the flexible hinges was always lower with respect to those from the fixed hinge model, this is not true for the first negative peak, which got worse for the more flexible hinge, K_θ=1.E0 Nm/rad. Figures 12(c) and 12(f) show that the increment of first negative peak for the flexible hinge model was given by the folding wing-tip having a phase shift of almost 180° with respect to the wing root bending moment trend.
  As consequence of this delay, the folding device generated a wing root bending moment contribution that was in-phase with the global wing root bending moment, which therefore was increased. Figures 12(b) and 12(e) show that, for K_θ=1.E06 Nm/rad this phase shift is lower, so a loads alleviation effect was achieved. This phase shift between the global wing root bending moment and the wing-tip rotation is the key element to enhance the load alleviation effect. In order to optimize the loads alleviation, the global wing root bending moment and the hinge deflection should be in phase at least for the first 2 peaks of the gust response.
  100 Kg wing-tip model. - For both the hinge stiffness values the folding tip device was able to alleviate the loads with respect to the fixed hinge model, especially for the more flexible hinge case where the wing root bending moment was very close to that of the baseline model. Figures 13(e) and 13(f) show that there was a small phase shift between the first wing root bending moment peak and the folding angle which was due to a very low contribution of the inertial forces. Figure 13(c) show that the aerodynamic forces generated by the wing-tip rotation balanced almost perfectly the loads given by the gust when a light wing-tip and a very flexible hinge spring were defined. This behavior confirms the efficiency in the loads alleviation since the wing-tip was almost unloaded during the gust event and so its contribution to the wing root bending moment was relatively small. The maximum folding angle achieved with such configuration was around 12.08°.

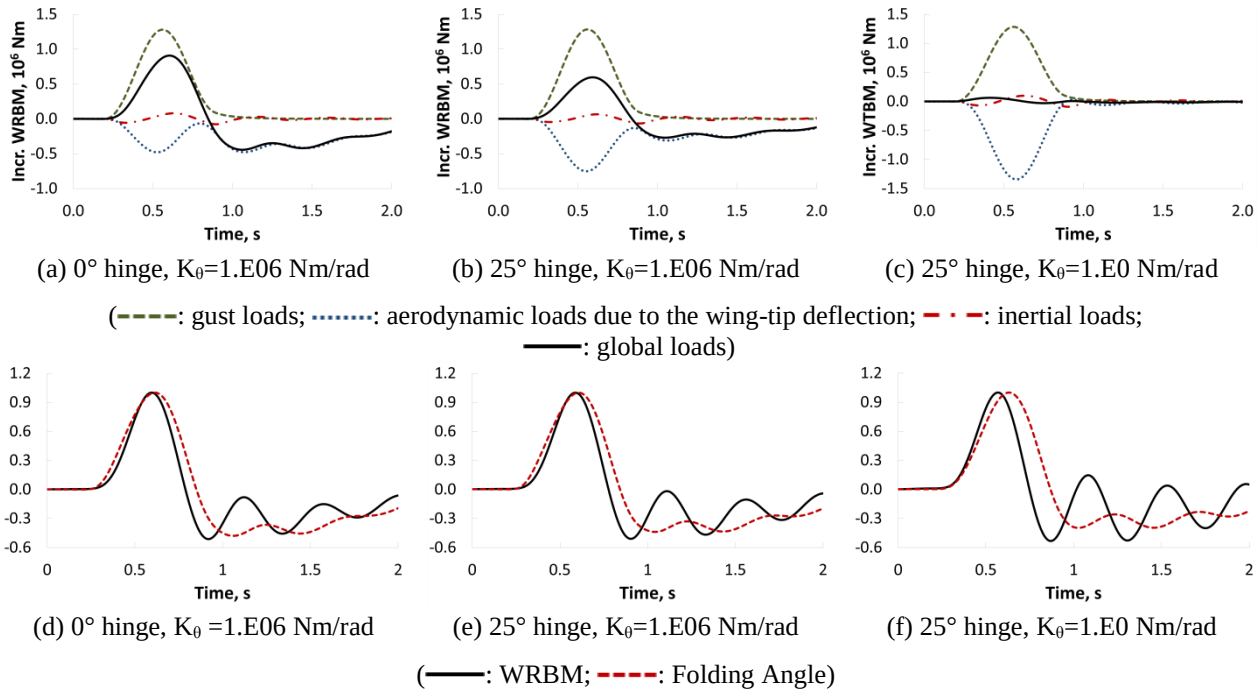

(a) 0° hinge, K_θ=1.E06 Nm/rad (b) 25° hinge, K_θ=1.E06 Nm/rad (c) 25° hinge, K_θ=1.E0 Nm/rad

(- - -: gust loads; ·····: aerodynamic loads due to the wing-tip deflection; — · —: inertial loads; ——: global loads)

(d) 0° hinge, K_θ =1.E06 Nm/rad (e) 25° hinge, K_θ=1.E06 Nm/rad (f) 25° hinge, K_θ=1.E0 Nm/rad

(——: WRBM; - - - -: Folding Angle)

Figure 13. 100 Kg Wing-Tip Model - Upper Plots: Aerodynamic And Inertial Loads Contributions Of The Wing-Tip To The Global Wing Root Bending Moment. Lower Plots: Global Wing Root Bending Moment VS Wing-Tip Folding Angle (normalised)

The dynamic responses of the models with a 0° hinge and 1.E06 Nm/rad spring stiffness, and with a 25° hinge and 1.E0 Nm/rad spring stiffness, were considered for several wing-tip mass configurations, ranging from 100 Kg to

943 Kg. Figure 14 shows the maximum and minimum incremental wing root bending moments over a range of gust lengths:

- 0° Hinge:
  By increasing the wing-tip mass there was a slight loads alleviation of the positive peaks due to an inertial relief effect, but no conclusion could be made for the negative loads which exhibited an irregular trend.
- 25° Hinge:
  A significant reduction for both positive and negative loads was achieved with a reduction in the wing-tip mass. Such an effect was more pronounced for the negative loads which were strongly affected by the wing-tip response delay and was minimized for low wing-tip masses.

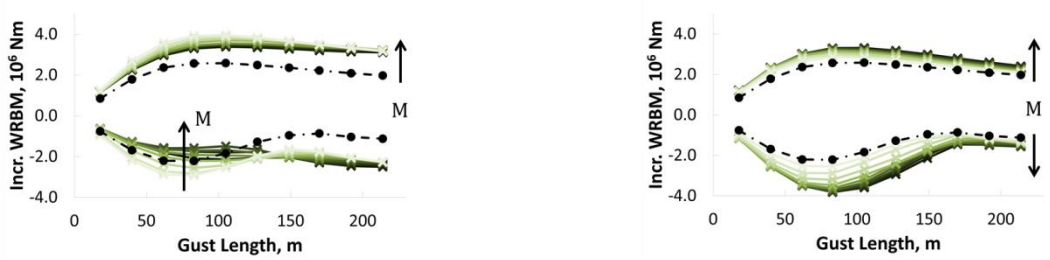

(a) 0° hinge, K_θ =1.E06 Nm/rad (b) 25° hinge, K_θ =1.E0 Nm/rad

Figure 14. WRBM Envelopes For Different Mass Configuration
(−●−:baseline model; ——:flexible hinge model
M=[100., 200., 300., 400., 500., 600., 700., 800., 943.] Kg)

3. Hinge Damping Effect

Further investigation was also made into the effect of adding a discrete damping element on hinge together with a spring. A hinge spring stiffness of 1.E06 Nm/rad for the 0° hinge model was used while 1.E0 Nm/rad and 1.E06 Nm/rad stiffness were used for the 25° hinge. The damping was varied between 1.E03 Nms/rad and 1.E06 Nms/rad. Figure 15 shows the maximum and minimum incremental wing root bending moments for the 0° and 25° hinges over a range of gust lengths for:

- 0° Hinge:
  943 Kg wing-tip model. - The introduction of a lumped damping element did not generate any load alleviation effect on the response of the model; the higher the damping, the greater the wing root bending moment for the flexible hinge and these values were close to that of the fixed hinge model.
  100 Kg wing-tip model. - The wing root bending moment was only slightly affected by the value of the damping element and remained almost unchanged with respect to that of the fixed hinge model.
- 25° Hinge:
  943 Kg and 100 Kg wing-tip models. - For the maximum loads, increasing the damping value led to the wing root bending moment trends tended to those of the fixed hinge model. For the minimum loads, the presence of a discrete damper sometimes generate loads which were higher than those of the fixed hinge model. This effect is due to the increasing of the delay between the wing root bending moment and the folding angle given by the damping element.

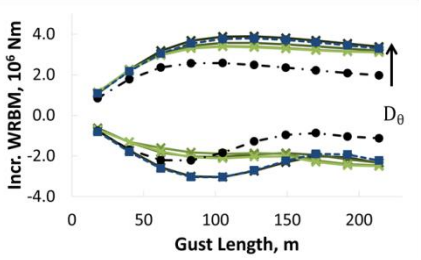

(a) 943 Kg wing-tip model, 0° hinge, K_θ =1.E06 Nm/rad

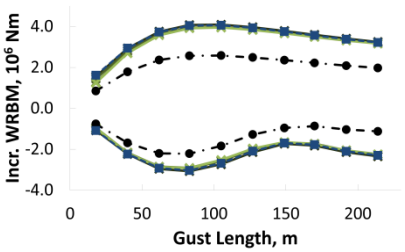

(b) 100 Kg wing-tip model, 0° hinge, K_θ=1.E06 Nm/rad

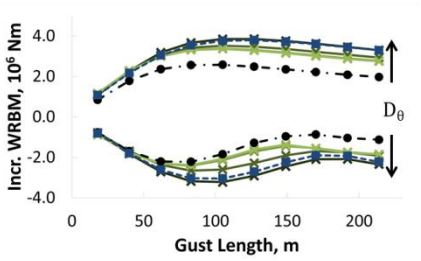

(c) 943 Kg wing-tip model, 25° hinge, K_θ=1.E06 Nm/rad

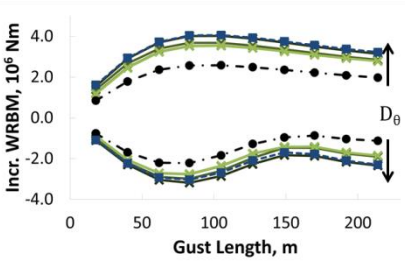

(d) 100 Kg wing-tip model, 25° hinge, K_θ=1.E06 Nm/rad

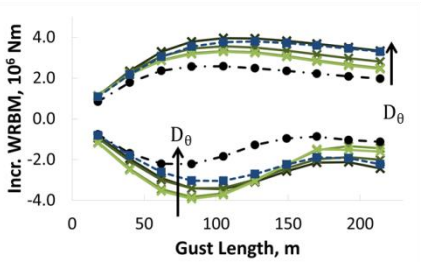

(e) 943 Kg wing-tip model, 25° hinge, K_θ=1.E0 Nm/rad

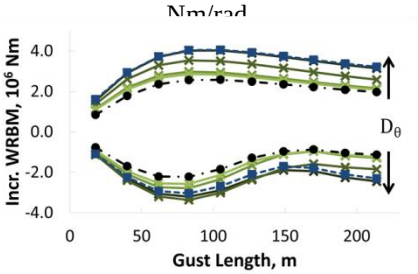

(f) 100 Kg wing-tip model, 25° hinge, K_θ=1.E0 Nm/rad

Figure 15. WRBM Envelopes For Different Hinge Damping Values
(-■-:fixed hinge model; −●−:baseline model; ——:flexible hinge model
D_θ=[1.E3, 1.E4, 1.E5, 1.E6] Nms/rad)

D. Continuous Turbulence Response Analysis

In this section, the dynamic response of the aircraft model with the folding wing-tips due to continuous turbulence was analyzed. Figures 16 and 17 show the root mean square values, RMS, of the wing root bending moment and the wing-tip folding angle. As before, several wing-tip mass, hinge spring stiffness and hinge angles were considered.

- Again, the baseline model was characterized by to the smallest loads level, as expected.
- 0° Hinge:
  The highest loads were experienced by the fixed hinge model. Some loads alleviation was achieved when a more flexible spring, 1.E06 Nm/rad, was used. For the unswept hinge, such alleviation effects were due to the aerodynamic damping and inertial forces generated by the wing-tip motion.
- 25° Hinge:
  The highest loads were experienced by the fixed hinge model for which a slight reduction of the loads was achieved by increasing the wing-tip mass. A reduction of the loads, with respect the fixed hinge case, was achieved with 1.E06 Nm/rad hinge spring stiffness, also in this case changing the folding device inertial properties introduced only a slight variation of the loads. However, when the more flexible hinge case was considered, changing the wing-tip mass led to a significant influence in the wing root bending moment. Minimum loads were achieved with a 100 Kg wing-tip configuration and a substantial change in the loads

was observed for mass cases between 200 Kg and 400 Kg, with even higher loads compared to the fixed hinge case; higher mass values led to a slight reduction of the loads, which were still significantly higher than the baseline model ones.

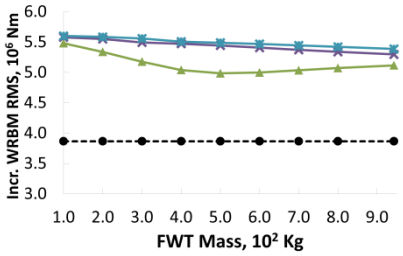

(a) Incremental WRBM, root mean square

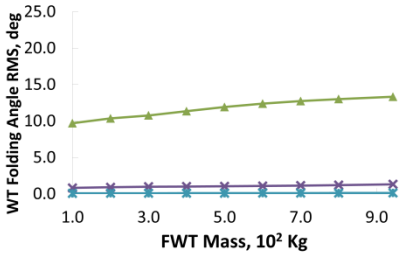

(b) Wing-Tip folding angle, root mean square

Figure 16. 0° Hinge Model, Continuous Turbulence RMS Analysis
(−●−:baseline model ; : K_0=1.E6Nm/rad; : K_0=1.E7Nm/rad; : K_0=1.E8Nm/rad)

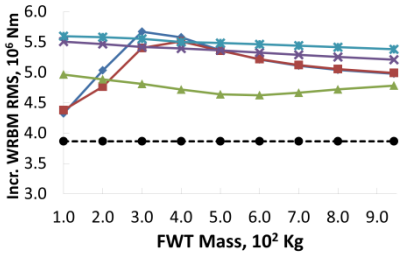

(a) Incremental WRBM, root mean square

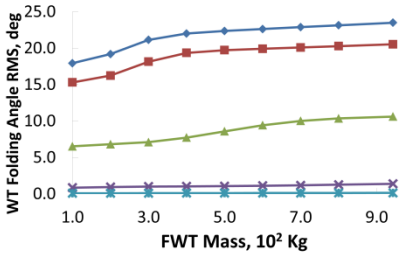

(b) Wing-Tip folding angle, root mean square

Figure 17. 25° Hinge Model, Hinge Model, Continuous Turbulence RMS Analysis
(−●−:baseline model ; : K_0=1.E0Nm/rad; : K_0=1.E5Nm/rad; : K_0=1.E6Nm/rad; : K_0=1.E7Nm/rad; : K_0=1.E8Nm/rad)

A better insight of such dynamic response is given by the power spectral density trends shown in Figs. 18 and 19. Figure 18 (a) shows the power spectral density of the wing root bending moment for the baseline model, the fixed hinge case and the flexible hinge cases for different hinge stiffness values and 100 Kg of wing-tip mass. The higher energy content of the aircraft frequency response is observed around 0.25 Hz and 2.23Hz, which represents respectively the short period and the first wing bending mode frequencies. The introduction of a flexible hinge enabled the energy content of the short period peak to decrease while the first wing bending mode peak increased, nevertheless this led to an overall reduction of RMS value of the wing root bending moment.

Time histories were produced by running time domain gust analyses using a gust profile time signal defined by combining a series of harmonic signals randomly shifted in phase as [6]

$$w_g(t) = \sum_{n=1}^{N_{sample}} 2\sqrt{\Phi(f_n)\Delta f_n}\cos(2\pi f_n t + \psi_n) \tag{6}$$

where $\Phi(f_n)$ is the value of the Von Karman PSD at a given frequency, Δf_n is the frequency step defined for the PSD discretization and ψ_n is the random phase. Such a random gust signal has same energy distribution, in frequency, of the Von Karman spectrum.

Figure 18(b) shows the time histories of the wing root bending moment for the baseline model, the fixed hinge model and the flexible hinge model with a spring stiffness of 1.E0 Nm/rad showing that the root

loads of the latter case were very close to the baseline model ones due to the efficient loads alleviation capability.

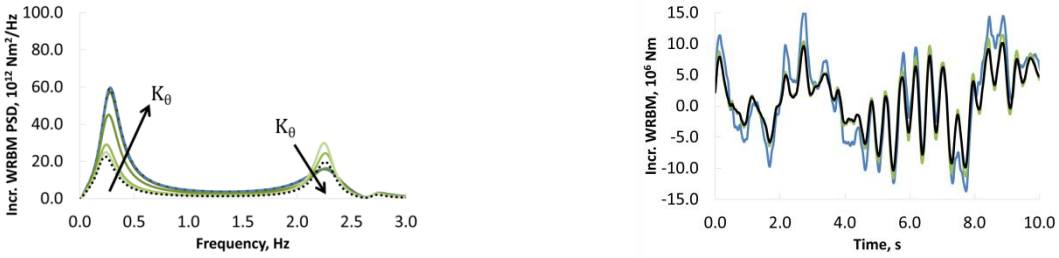

(a) WRBM PSD

(b) WRBM time histories
(K_θ= 1.E0 Nm/rad, M=100 Kg)

Figure 18. 25° Wing Root Bending Moment PSD and Time Histories – Hinge Stiffness Effect (– – – –:fixed hinge model; ·····:baseline model; ——:flexible hinge model K_θ=[1.E0, 1.E5, 1.E6, 1.E7, 1.E8] Nm/rad and M=100 Kg)

In Fig. 19 (a) the power spectral density trend of the wing root bending moment for different wing-tip mass and a fixed hinge spring stiffness of 1.E0 Nm/rad are shown. The second PSD peak around the first wing bending mode frequency was strongly influenced by the wing-tip mass variation. The highest values were obtained for the 300 Kg and 400 kg configurations, confirming the trend reported in Fig. 17(a). No variations were observed for the first peak. Figure 19(b) shows the time histories of the wing root bending moment when a 300 Kg wing-tip and a 1.E0 Nm/rad spring were defined, a significant increment in the loads with respect the baseline model was observed; however, the results for 100 kg tip were still close to the baseline model.

Figure 20 shows the variation of the first wing-tip and first wing bending mode frequencies when a hinge spring stiffness of 1.E0 Nm/rad and several mass cases were considered. Such modal frequencies account for the aeroelastic effects and were evaluated by investigating the frequencies of those modes from a matched flutter analyses at a Mach value of 0.6, an altitude of 25000 ft and a flight speed of 185.8 m/s. The excitation introduced by the random gust led, as expected, to peaks of the wing root bending moment PSD for frequencies close to the first wing bending moment for all the mass cases. It has been demonstrated that the wing-tip could be considered a quasi-uncoupled dynamic system, with respect the main airframe, when low spring stiffness and low wing-tip mass were defined. Figure 20 shows that for a wing-tip mass of 100 Kg the wing-tip mode has a frequency of 2.84 Hz, which is higher than that the wing bending mode, 2.26 Hz, allowing the wing-tip to be fast enough to react to the gust loads. The latter were giving a peak of the wing root banding moment PSD at 2.25 Hz. A wing-tip mass of 200 Kg led to a wing-tip mode frequency of 2.23 Hz and a wing bending mode frequency of 2.22 Hz, which means that the frequency giving a peak of the wing root bending moment PSD was close to the aeroelastic resonant frequency of the wing-tip. This effect led to a consequent a phase shift of the response of folding device with respect to the external excitation of 90°. For the 300 Kg and 400 Kg mass cases, the wing-tip natural frequency was even lower leading to a higher phase shift up to 180° and the PSD peak was now at a frequency higher than the wing-tip resonance. The increment of the wing-tip phase shift resulted in an increment of the loads experienced by the aircraft. Higher mass cases led to lower PSD peaks, around the frequency of the first wing-tip bending mode, but also to increment of the PSD in lower frequency bands, indicating a stronger inertial coupling between the main airframe and the wing-tip.

For all the structural configurations the loads due to continuous turbulence were always higher than the baseline model however, the results for a low stiffness low mass wing-tip showed loads only slightly worse. It should be noted that the responses are very sensitive to the wing-tip mass values. Such effect was due to the fact the Von Karman gust profile excited higher frequency components of the aeroelastic system, with respect the "1-cosine" excitation.

Such trend highlighted a limitation in the loads alleviation performance of the proposed hinge device

when higher frequency excitations had to be alleviated. It is so fundamental to design the folding device such as the first wing-tip mode aeroelastic frequency is high enough to allow an efficient alleviation of the external gust loads. This can be achieved either by reducing the wing-tip mass or by increasing the hinge sweep angle which would reflect into an increment of the aerodynamic stiffness of the wing-tip.

- As regards the mean wing-tip deflection angles, reported in Figs. 16(b) and 17(b), the results showed that the lower was the hinge spring stiffness and the higher was the wing-tip mass, the higher was the wing-tip mean folding angle.

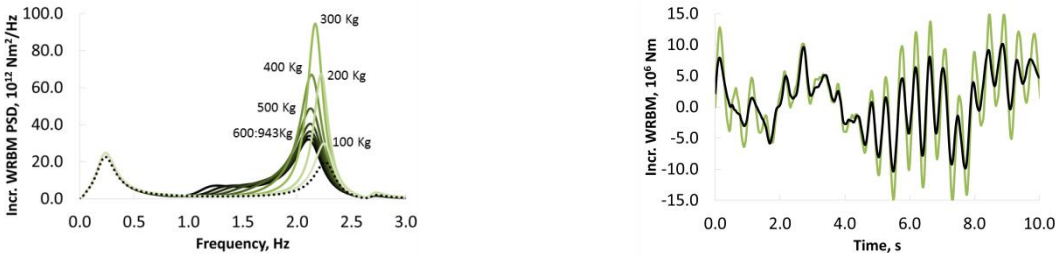

(a) WRBM PSD

(b) WRBM time histories
(K_0= 1.E0 Nm/rad, M=300 Kg)

Figure 19. 25° Wing Root Bending Moment PSD and Time Histories – Wing-Tip Mass Effect
(·····:baseline model; ——:flexible hinge model
M=[100., 200., 300., 400., 500., 600., 700., 800., 943.] Kg and K_0= 1.E0 Nm/rad)

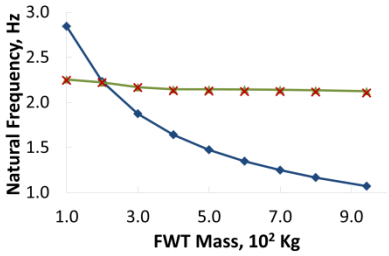

Figure 20. First Wing-Tip and First Wing Bending Modes Aeroelastic Natural Frequencies, at M=0.6, h=25000 ft and V=185.8 M/s
(◆—: 1st wing-tip mode; ▲—: 1st wing bending mode; ✖: WRBM PSD peak frequency)

V. Conclusions

A preliminary investigation on the effects of using folding wing-tips as loads alleviation device was performed using a numerical aeroelastic model of a typical commercial jet aircraft. A wing-tip device was connected to the wings with an elastic hinge, increasing the span of 25%, and the effect of varying the hinge stiffness, damping, hinge orientation and wing-tip mass, on the static loads, gusts loads and flutter behavior was investigated. All results were related to the loads acting on a baseline model which consisted of the aircraft without wing-tips.

The static analyses showed that the response of the model was highly influenced by the orientation of the hinge and that no loads alleviation effect was observed for the streamwise hinge case. The greater the hinge angle with respect to the free stream direction, and the lower the hinge spring stiffness and wing-tip mass, the greater the loads alleviation due to the resulting nose down twist of the wing-tip. For the case considered in the static trim analyses, a 25° hinge with low hinge stiffness gave wing root loads that were reduced by nearly 30% compared to rigid hinge case and gave loads of just 4.36% higher than the reference model with no wing-tips, despite the total span increasing by 25%.

From the flutter analyses was observed that, when a 25° hinge was defined, a low wing-tip mass were beneficial for the aeroelastic stability both for flexible and fixed hinges. A significant reduction in the flutter speed was observed when a flexible hinge with a high wing-tip mass was defined. The 0° hinge model was instead

characterized by very high flutter speeds for all the wing-tip mass hinge spring combinations.

The deterministic gust response analyses highlighted that it was possible to obtain significant loads reductions with a swept hinge angle, a reduced wing-tip weight and a low hinge spring stiffness. Detailed studies showed how the interactions between the inertia, elastic and aerodynamic forces worked favorably in order to enhance the loads alleviation capability.

The random gust analyses confirmed that good loads alleviation could be achieved with a swept hinge, low wing-tip mass and very small hinge spring stiffness. However a higher sensitivity of the loads alleviation capabilities with respect to the wing-tip mass was observed.

Through proper design of the wing-tip device it will be possible to increase the wing aspect ratio with little, if any, increase in the internal loads experienced by the aircraft, leading to better aerodynamic efficiency, or simply to reduce the loads and hence the weight on existing platforms. Further work is required to improve the modeling and the design of the hinge device and to develop an experimental prototype.

VI. Acknowledgments

The research leading to these results has received funding from the European Community's Marie Curie Initial Training Network (ITN) on Aircraft Loads Prediction using Enhanced Simulation (ALPES) FP7-PEOPLE-ITN-GA-2013-607911 and also the Royal Academy of Engineering. The partners in the ALPES ITN are the University of Bristol, Siemens PLM Software and Airbus Operations Ltd.

References

1. Khodaparast H.H, Cooper J.E., Rapid Prediction of Worst Case Gust Loads Following Structural Modification, AIAA Journal, Vol. 52, No. 2 (2014), pp. 242-254.

2. Hodigere Siddaramaiah V., Calderon D. E., Cooper J.E., Wilson T., Preliminary Studies in the use of Folding Wing-Tips for Loads Alleviation, Royal Aeronautical Society Applied Aerodynamics Conference, Bristol, 2014.

3. Albano E., Rodden W.P., "A Doublet-Lattice Method for Calculating Lift Distributions on Oscillating Surfaces in Subsonic Flows", AIAA Journal v7 n2 1969 pp 279-285.

4. Rodden W.P., Johnson E.H. , "MSC/NASTRAN Aeroelastic Analysis' User's Guide", MSC Software, USA, 1994.

5. Wright J.R., Cooper J.E., Introduction to Aircraft Aeroelasticity and Loads, John Wiley, 2007.

6. Hoblit F. M., "Gust loads on aircraft: concepts and applications", AIAA, 1988.

7. Di Vincenzo F.G., Castrichini A., "User's Guide of Hybrid Static Aeroelasticity Toolkit", MSC Software, 2013.